ELSEVIER

Ceramics International 32 (2006) 173–179

CERAMICS INTERNATIONAL

www.elsevier.com/locate/ceramint

Ceramic formulations prepared with industrial wastes and natural sub-products

F. Raupp-Pereira [a], D. Hotza [b], A.M. Segadães [a], J.A. Labrincha [a,*]

[a] *Ceramics and Glass Engineering Department, CICECO, University of Aveiro, 3810-193 Aveiro, Portugal*
[b] *Chemical Engineering Department, Federal University of Santa Catarina, 88040-900 Florianópolis-SC, Brazil*

Received 13 September 2004; received in revised form 12 December 2004; accepted 29 January 2005
Available online 24 March 2005

Abstract

This work describes the studies carried out with various industrial wastes and natural sub-products based on the SiO_2–Al_2O_3–CaO system, aimed at producing ceramic products of industrial interest. The physical and chemical characterization of the waste materials is reported and their thermal behaviour is described. Several mixtures were prepared and fired at different temperatures. Compositional evolution was assessed by X-ray diffraction and fluorescence and the sintered samples were characterised in terms of density and mechanical strength. For comparison, similar compositions based on high purity grade commercial reagents were also investigated. The presence of impurities in the former waste materials induces changes on functional properties (e.g. refractoriness). However, those variations are easily predicted and can be accounted for.

Keywords: E. Refractories; Mortars; Industrial wastes

1. Introduction

The continuous demand for higher productivity indices in the global competitive world has led to a fast decrease of the available natural resources and, at the same time, to the generation of a high volume of rejects or sub-products, most of them not directly recyclable. Mineral extraction itself is a good example of reject production [1]. Industrial processes like aluminium anodising and powder surface coating are highly water consuming and, in the end, a huge flow of wastewater has to be treated, leading to the formation of high amounts of sludge [2]. Even the basic activity of water filtration/clarification for human consumption generates a significant volume of sludge [3]. In general, the composition of a specific waste product reflects its source, showing varied levels of contamination depending on the processing/conditioning methods used.

Traditionally, waste products are disposed of as soil conditioners or in land filling. However, there might be reusing or recycling alternatives that should be investigated and eventually implemented [4–9]. Other than the usual limited incorporation in ceramic bodies with a given shape and size, expanded clays, cement and refractory mortars offer increased capabilities for high incorporation levels of rejects, as the final products are powders [10–12]. In particular, cement fabrication also involves a huge consumption of natural raw materials (e.g. limestone and clay) and recently new waste-based formulations have been tried. The so-called eco-cement [13] is the best example, amongst several known cases of minor incorporation of wastes, such as fly ash and slag [14–16].

In terms of chemical composition, the dominant oxide in the great majority of waste materials is silica (SiO_2), closely followed by alumina and lime (Al_2O_3, CaO), and finally by fluxing oxides (alkalies and iron). If a prediction is needed, of the effect and/or the role of the waste material within a given process or product, it can be looked for in the system SiO_2–Al_2O_3–CaO–(Na_2O, K_2O, iron oxide).

* Corresponding author. Tel.: +351 234370250; fax: +351 234425300.
E-mail address: jal@cv.ua.pt (J.A. Labrincha).

0272-8842/$30.00
doi:10.1016/j.ceramint.2005.01.014

On the other hand, cements, and hydraulic cements in particular, can also be described in terms of their SiO_2, Al_2O_3 and CaO contents and the phase equilibrium diagram of that system is often used in the study of cement mineralogy and compatibility relationships. For high temperature applications (e.g. refractory castables) or for uses in aggressive media (e.g. sulphates), calcium aluminate cements are preferred to the conventional, calcium silicate-based, Portland cement. Their content in alumina is the distinguishing parameter and the refractoriness directly reflects it.

Although in normal industrial operating conditions thermodynamic equilibrium is usually not reached, the equilibrium phase diagram of the relevant system can still be used to foresee the reactions tendency to completion and be of great assistance while making educated choices of compositions and processing parameters.

This work describes the attempts to define the compositions of waste-based mixtures and the corresponding processing conditions suitable to the production of refractory and/or cement-like materials. For comparison, and to clarify the effect of minor components, present in the waste materials, on the final products properties, similar compositions were also prepared with commercial high purity grade raw materials and used as standard samples.

2. Experimental procedure

Four waste materials were selected and characterised, namely, (i) Al-rich anodising sludge (A-sludge), (ii) sludge from the filtration/clarification of potable water (W-sludge), (iii) sludge generated in marble sawing processes (M-sludge), and (iv) foundry sand (F-sand). The A-sludge was firstly calcined at 1400 °C and milled (6.5 μm final average particle size) (A-calc); the foundry sand was also milled and sieved through 75 μm; the other materials were used in the as-received condition. The alternative commercial high purity grade raw materials used were: the Alcoa CT3000 alumina, the Calcitec M1 calcite, and the Sibelco P 500 sand. The characterisation included chemical composition, determined by X-ray fluorescence (XRF, Philips X'UNIQUE II), thermal behaviour (DTA and TGA, SETARAM—LabSys) and particle size distribution (Beckman Coulter LS 230). The detailed characterisation of A- and W-sludges can be found elsewhere [2,12,17,18].

After drying at 110 °C, six different mixtures of the various wastes (C1–C6) were prepared by dry mixing/milling (for 30 min, in a porcelain jar with alumina grinding balls) and the resulting loose powders were calcined at selected temperatures (10 °C/min heating and cooling rates, 1 h soaking at the chosen temperature). For comparison, compositions C1 and C3 were also prepared with the commercial high purity grade raw materials mentioned above (standard samples C1-P and C3-P). Powder density was determined by He picnometry (Gemini II 2370). The crystalline phases formed were identified by X-ray diffraction (XRD, Rigaku Geigerflex D/max—Series).

Powders of the raw mixtures were also used to prepare uniaxially pressed test bars, which were sintered at the same temperature used in the calcination of the corresponding powder mixture. Flexural and compressive strengths of the sintered bars were measured (Shimadzu—autograph AG-25TA) and their apparent density was determined using Archimedes method in Hg. Polished surfaces of the sintered microstructures were observed by Scanning Electron Microscopy (SEM, HITACHI S-4100), after etching (5 min in 0.1N HF) and carbon coating.

3. Results and discussion

Table 1 shows the chemical compositions (wt.%) of all the materials used, as determined by XRF.

Upon calcination, the hydroxides and sulphates (calcium, sodium and aluminium) present in the A-sludge decompose and pure Al_2O_3 (α and β) is obtained [18].

The W-sludge consists basically of calcium and aluminium hydroxides and sulphates and its moisture level can reach 82 wt.%. In the dried material, the maximum particle size is circa 100 μm. Its full characterisation is detailed elsewhere [3].

M-sludge is basically composed of calcite, as denoted by the CaO content (54.5 wt.%), by the loss on ignition (43.8%) and by the strong endothermic decomposition peak (DTA) at about 900 °C (Fig. 1). It can be considered as a rather pure raw source for calcite, since stoichiometric purity corresponds to 55.9 wt.% CaO. Its fineness is well illustrated by the low fraction (6.4 wt.%) of particles retained at the 75 μm sieve. In the as-received state, the water content is about 17 wt.% and a drying operation is not required.

Table 1
Average chemical composition (XRF, wt.%) of wastes and commercial raw materials (n.d., not determined; presumed, <0.5%)

Wastes	Al_2O_3	SiO_2	Fe_2O_3	CaO	Na_2O	K_2O	MgO	TiO_2	ZnO	MnO	LoI
A-calc	89.8	1.80	2.87	4.32	0.61	0.09	0.22	0.10	0.08	0.10	–
W-sludge	10.7	12.4	4.39	33.7	0.05	0.75	1.01	0.29	0.13	0.35	35.0
M-sludge	0.14	0.63	0.24	54.5	0.01	0.11	0.30	0.02	0.01	0.01	43.0
F-sand	0.20	97.5	1.12	0.22	0.02	0.26	0.03	0.20	0.02	0.02	0.22
Alumina	99.3	0.17	0.37	0.02	0.00	0.04	0.00	0.06	0.01	0.01	n.d.
Calcite	0.00	0.00	0.07	55.8	0.00	0.01	0.22	0.01	0.00	0.00	43.9
Sand	0.10	99.6	0.06	0.07	0.05	0.00	0.07	0.01	0.00	0.00	n.d.

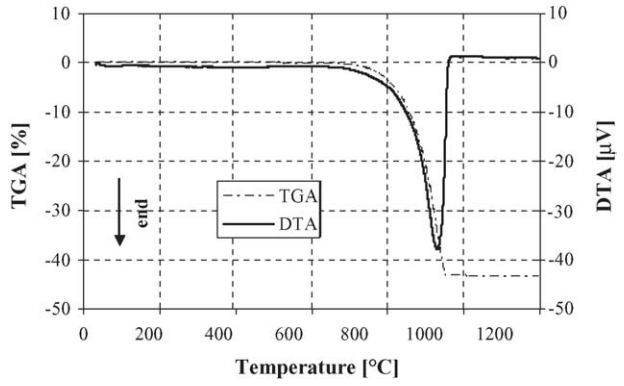

Fig. 1. DTA and TGA curves of dried M-sludge, showing the dissociation of carbonates.

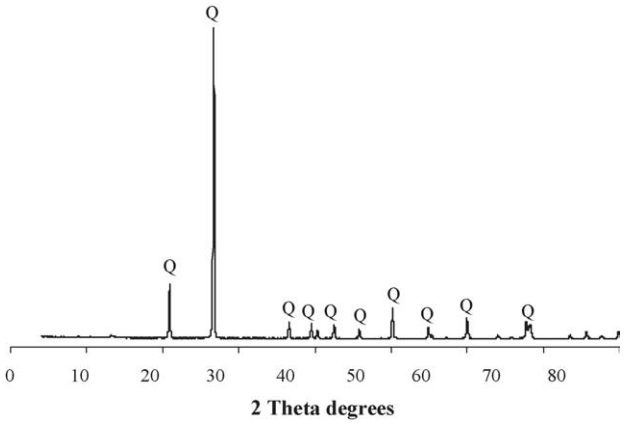

Fig. 2. XRD pattern of the foundry sand, showing the characteristic peaks of quartz.

Quartz is the only crystalline phase detected in the F-sand (Fig. 2), which contains 97.5 wt.% SiO_2. The total weight loss upon firing at 1200 °C is ∼1%, which can be attributed to the organic additives (binders, plasticizers) used for mould shaping. Maximum particle size can reach 1 mm, requiring grinding prior to mixing with other materials.

In terms of major components, W-sludge is obviously a ternary composition ($SiO_2 + Al_2O_3 + CaO$), whereas the other three materials could, in good approximation, be considered ''single component'' wastes. The composition diagram of the SiO_2–Al_2O_3–CaO ternary system (S–A–C, in shorthand notation) can be used to represent all four materials, as shown in Fig. 3. Given that the ''single component'' wastes lie very close to the apexes of the diagram, essentially any composition within the S–A–C system could be prepared with those three materials and the W-sludge itself can be reproduced with them.

Bearing in mind the general composition range of common and high-alumina mortars and cements, six compositions were prepared with the industrial wastes, as shown in Table 2 and also in Fig. 3. The selected calcination temperatures were chosen based on the phase compatibility relationships in the relevant area of the S–A–C ternary

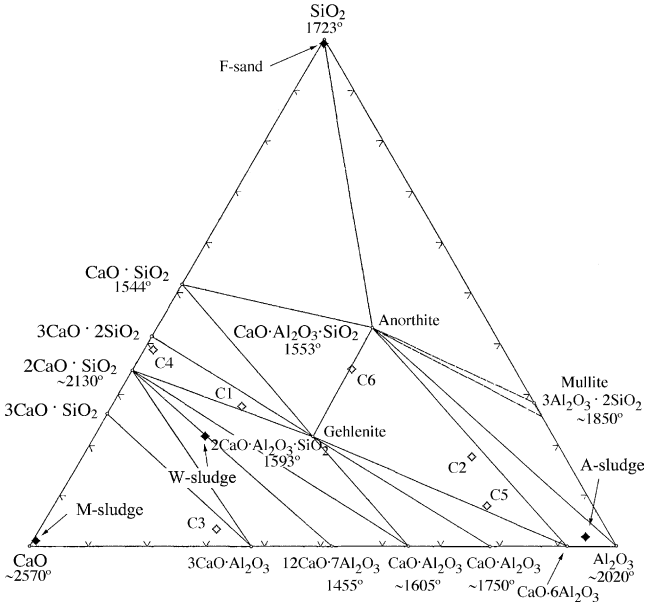

Fig. 3. Location in the composition diagram of the SiO_2–Al_2O_3–CaO ternary system, of the wastes and the compositions investigated.

Table 2
Proportions of starting materials in the mixtures investigated (wt.%)

Mixture	A-calc	W-sludge	M-sludge	F-sand	Alumina	Calcite	Sand
C1	16.0	9.0	57.0	18.0	–	–	–
C2	58.0	32.0	–	10.0	–	–	–
C3	20.0	10.0	70.0	–	–	–	–
C4	–	8.0	67.0	25.0	–	–	–
C5	70.0	5.0	20.0	5.0	–	–	–
C6	30.0	20.0	25.0	25.0	–	–	–
C1-P	–	–	–	–	16.0	64.2	19.8
C3-P	–	–	–	–	19.8	78.1	2.1

system. Fig. 4 and Table 3 show those temperatures and the crystalline phases identified after firing (XRD).

Mixtures C1 and C4 (Portland cement-type) belong to the compatibility triangle C_2S–C_3S_2–C_2AS (Fig. 5), in which melting begins at 1315 °C. Both lie in the C_2S primary phase field and were fired at 1350 °C. If in equilibrium at the firing temperature, they should contain $C_2S + C_2AS$ (C1) and C_2S+C_3S_2 (C4), the secondary phase being dominant. Fig. 4 shows that, indeed, that is the tendency expressed by the compositions.

Mixtures C2 and C5 (refractory cement-type) belong to the compatibility triangle CA_6–C_2AS–CAS_2 (Fig. 6). In both, initial melting occurs at 1380 °C, but they lie in different primary phase fields, namely, corundum (C2) and CA_6 (C5). After melting begins, both mixtures contain one liquid phase in equilibrium with two solids: $CA_6 + CAS_2$ for C2, up to ∼1490 °C, and $CA_6 + C_2AS$ for C5, up to 1475 °C. A detailed study of their equilibrium melting behaviour shows that, between ∼1490 and ∼1620 °C, mixture C2 contains a liquid phase in equilibrium with only one solid phase, viz. CA_6, whereas mixture C5, between 1475 and ∼1600 °C, contains a liquid phase in equilibrium with

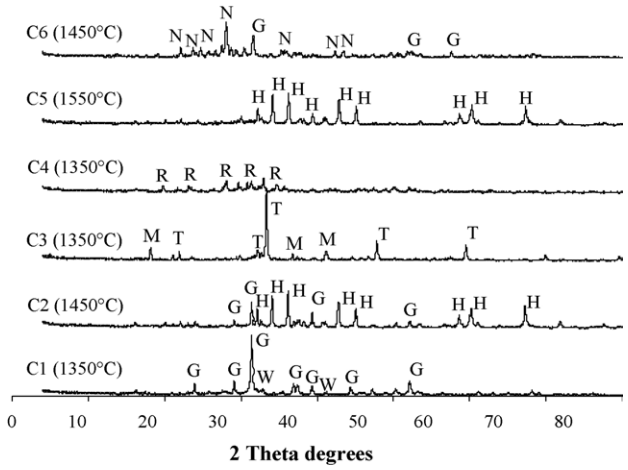

Fig. 4. XRD patterns of heat treated mixtures, showing the characteristic peaks of: gehlenite (G, C_2AS), hibonite (H, CA_6), calcium silicate (W, C_2S), tricalcium aluminate (T, C_3A), meyenite (M, $C_{12}A_7$), rankinite (R, C_3S_2) and anorthite (N, CAS_2).

$CA_6 + CA_2$. Hence, the firing temperatures chosen were 1450 °C for C2 and 1550 °C for C5. Fig. 4 shows that, while mixture C5 might have reached equilibrium (only CA_6 was detected, but the expected small amount of CA_2 might be below XRD detection limit), mixture C2 still has not reached it. It is possible that the reactions with quartz are sluggish, even in the presence of a liquid phase. Thus, alumina reacts first with lime, to form CA_6, and then with silica, to form C_2AS. Anorthite (CAS_2) would be the last solid to appear. Hence, mixture C2, with higher silica content, contains CA_6, but also C_2AS, which is a non-equilibrium phase.

Mixtures C6 and C3 were purposefully chosen outside the general composition range of interest and are used as a comparison tool. Mixture C6 lies on the Alkemade line between CAS_2 and C_2AS (melting begins at 1385 °C), on the CAS_2 primary phase field (Fig. 6). It was fired at 1350 °C and both phases (CAS_2 and C_2AS) were detected in the X-ray diffractogram (Fig. 4).

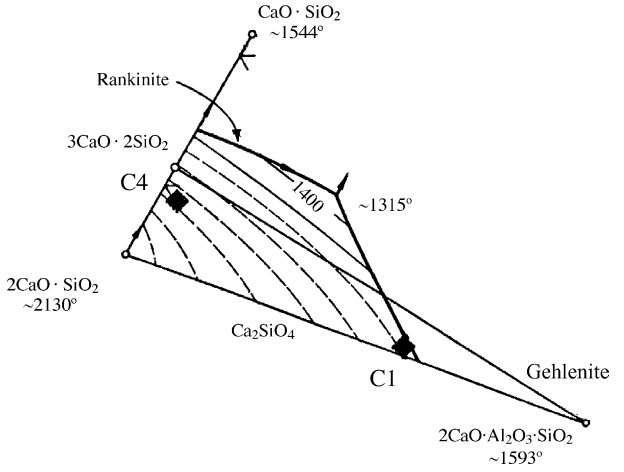

Fig. 5. Compatibility triangle C_2S–C_3S_2–C_2AS ($2CaO·SiO_2$–$3CaO·2SiO_2$–$2CaO·Al_2O_3·SiO_2$), showing the location of mixtures C1 and C4 in the C_2S primary phase field.

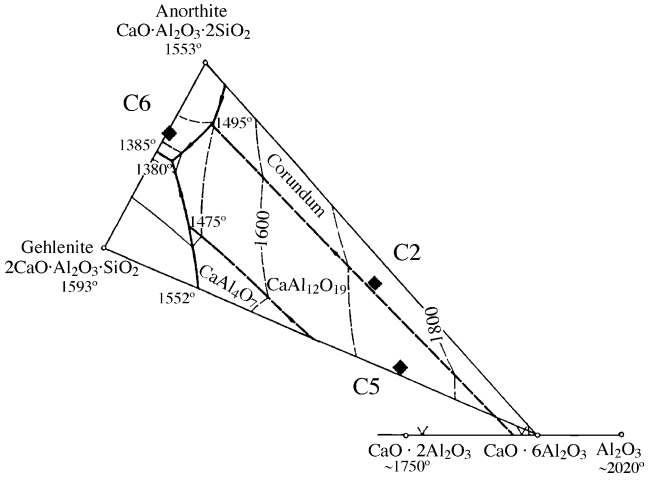

Fig. 6. Compatibility triangle C_2AS–CAS_2–CA_6 ($2CaO·Al_2O_3·SiO_2$–$CaO·Al_2O_3·2SiO_2$–$CaO·6Al_2O_3$), showing the location of mixtures C2, C5 and C6.

Mixture C3 lies in the primary phase field of lime (CaO), in the compatibility triangle C–C_3S–C_3A (Fig. 7), within which melting begins at 1470 °C. The composition was chosen so that, in the solid state, calcium aluminate (C_3A) is the major phase, both lime and calcium silicate (C_3S) being minor phases (~7–10%, calculated by the lever rule). The heat treatment temperature selected was 1350 °C, i.e. below initial melting. The diffraction pattern shown in Fig. 4 suggests that equilibrium at the sintering temperature is not fully established. Mixture C3 contains C_3A, the expected major crystalline phase, but the presence of $C_{12}A_7$, which is compatible with C_3A in the neighbouring compatibility triangle, gives some indications about the formation mechanism of the aluminates: C_3A is formed at the expenses of other alumina-richer aluminates.

Thus, the major crystalline phases identified were those predicted by the ternary S–A–C diagram, bearing in mind the expected departure from equilibrium. The presence of alien components, which mostly contributes to lowering the initial melting temperatures and, in doing so, promotes

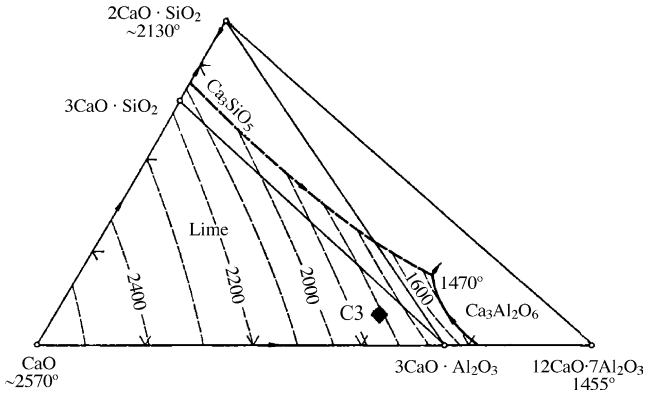

Fig. 7. Compatibility triangle C–C_3S–C_3A (CaO–$3CaO·SiO_2$–$3CaO·Al_2O_3$), showing the location of mixture C3 and the neighbouring compatibility triangles.

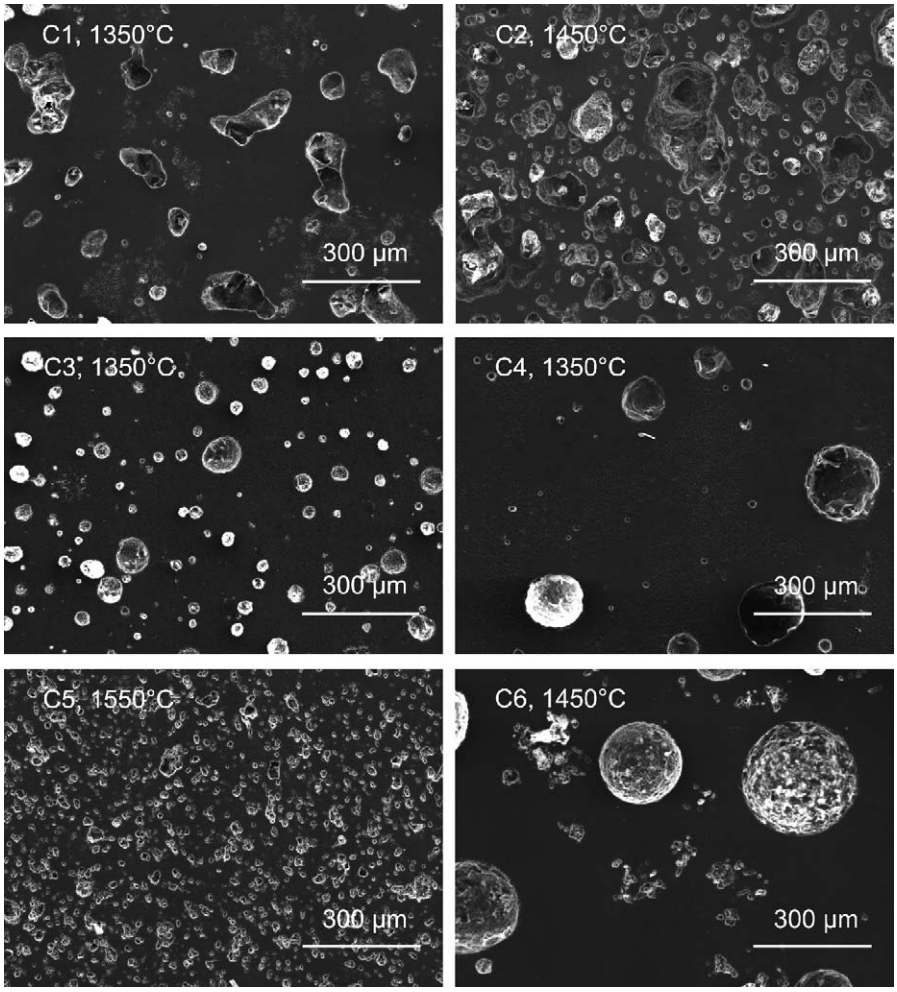

Fig. 8. SEM micrographs of the polished surfaces of sintered samples.

sintering and the establishment of equilibrium, does not seem to have a very remarkable effect.

Table 3 summarises the relevant characteristics of both calcined powders and sintered samples. The values of fired body mechanical strength and relative density reflect the combined effect of composition, sintering temperature and departure from initial melting temperature.

Compositions C2 and C5, lying in the more refractory area of the diagram (Fig. 3) are richer in alumina and require higher sintering temperatures to reach significant densification levels. They have the same low initial melting temperature and were fired well above it (Table 3). In this case, the role of the liquid phase present at the sintering temperature is clearly noticeable and, because the estimated amount of that liquid is higher for C2 (∼20%) than for C5 (∼9%), densification of C5 and its mechanical strength are lower than those of C2.

By contrast, compositions C1 and C4 were fired just above the initial melting temperature and both contain little liquid at the firing temperature. Nevertheless, these compositions are less refractory and reach comparatively high relative densities. Again, the low bending strength of composition C1 reveals the small amount of a bonding phase.

Sintering of compositions C3 and C6 was carried out at a temperature below liquid formation and their mechanical strength is low. Hence, the comparatively high relative densities reached (Table 3), are probably due to better particle packing of finer powders.

Fig. 8 shows microstructure details of the sintered samples. In particular, differences in porosity, hence in relative density, are clearly noticeable.

One composition in each group was studied in more detail, to investigate the departure from equilibrium, and the effect of impurities (high purity grade raw materials).

Composition C2 was selected to investigate the effect of sintering parameters (temperature and time) on the tendency towards equilibrium. The diffraction patterns in Fig. 9 show the phase changes in mixture C2 as a function of the sintering temperature and dwell time. As expected, departure from equilibrium decreases as the sintering temperature increases (Fig. 9A). At 1350 °C, C2 still contains residual alumina (A), together with hibonite (CA_6) and gehlenite (C_2AS), but no anorthite (CAS_2) is detected.

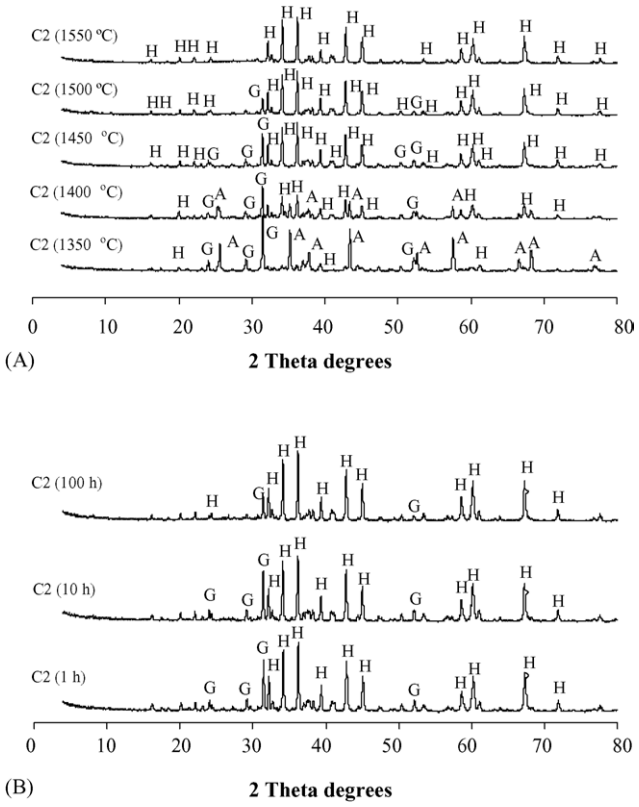

Fig. 9. XRD patterns showing the phase development in composition C2: (A) effect of sintering temperature (1 h at the temperature shown); and (B) effect of dwell time at 1450 °C. Characteristic peaks of gehlenite (G, C_2AS), hibonite (H, CA_6) and alumina (A) are shown.

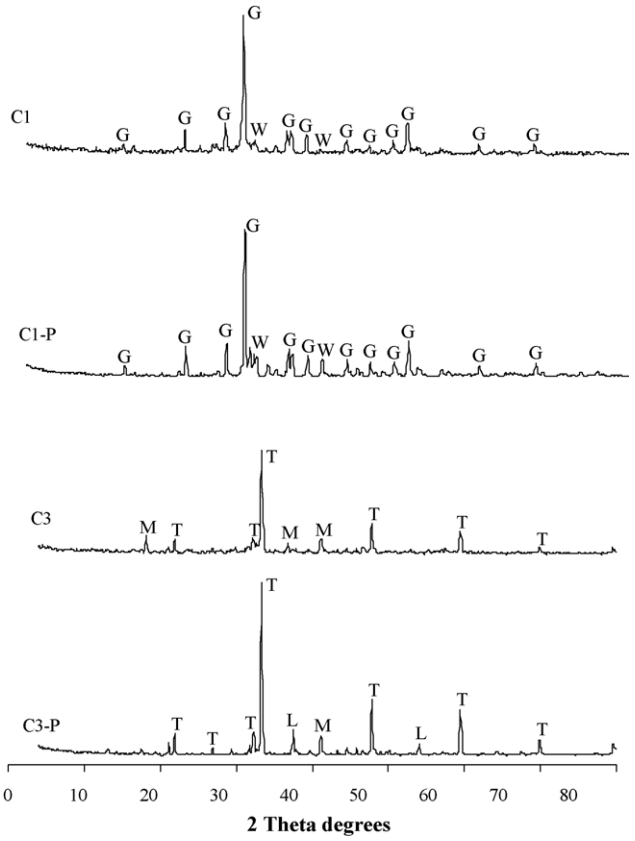

Fig. 10. Effect of raw materials in the phase development upon sintering: compositions C1 and C3 prepared with waste materials and with commercial high purity grade raw materials (C1-P and C3-P). Characteristic peaks of gehlenite (G, C_2AS), calcium silicate (W, C_2S), tricalcium aluminate (T, C_3A), meyenite (M, $C_{12}A_7$) and lime (L, CaO) are shown.

With the rise in temperature (1400 °C), residual alumina content decreases. From 1450 up to 1550 °C, CA_6 content increases at the expenses of that of C_2AS. At 1550 °C the only crystalline phase detected is CA_6, which is in clear agreement with the dictates of the phase diagram (Fig. 6). Increasing the dwell time (from 1 to 100 h, at 1450 °C) also improves the equilibrium conditions (Fig. 9B), as was to be expected. However, even after 100 h at the temperature, gehlenite can still be detected and there are no signs of anorthite. These results clearly show that rising the firing temperature is more effective than increasing the dwell time, in order to approach equilibrium.

As an attempt to discriminate the effect or minor constituents or impurities in waste-based materials, new compositions C1 and C3 were prepared using high purity grade reagents (standard samples C1-P and C3-P). The diffraction patterns of the new C1-P and C3-P formulations, shown in Fig. 10, compare reasonably well with those of the original C1 and C3 mixtures. The main difference occurs between C3 and C3-P and is due to the presence of free CaO in the last composition. This phase is predicted from the analysis of the equilibrium phase diagram but is only present in the standard sample due to its lower reactivity (no fluxing impurities). As a consequence, the sintered material is weaker than the corresponding waste-based sample (C3). A similar tendency is observed between C1 and C1-P, as can be

Table 3
Relevant characteristics of calcined powders and sintered samples

Property	C1	C2	C3	C4	C5	C6
Calc./sinter. temperature (°C)	1350	1450	1350	1350	1550	1350
First melting temperature (°C)	1315	1380	1470	1315	1380	1385
Temperature above melting (°C)	+35	+70	−120	+35	+170	−35
Major phases (XRD)	C_2AS, C_2S	CA_6, C_2AS	C_3A, $C_{12}A_7$	C_3S_2, C_2S	CA_6	CAS_2, C_2AS
Powder density (g/cm^3)	2.920	2.931	2.703	2.807	3.290	2.747
Apparent density (g/cm^3)	2.66	2.62	2.62	2.38	2.14	2.45
Relative density (%)	91	89	97	85	65	89
Flexural strength (MPa)	54.8	107.8	–	–	59.6	–
Compressive strength (MPa)	121.0	136.8	64.0	–	90.8	113.1

Table 4
Relevant characteristics of calcined powders and sintered standard samples

Property	C1-P	C3-P
Major phases (XRD)	C_2AS, C_2S	C_3A, $C_{12}A_7$, CaO
Powder density (g/cm^3)	2.727	2.468
Apparent density (g/cm^3)	2.35	1.91
Relative density (%)	86	77
Flexural strength (MPa)	33.6	–
Compressive strength (MPa)	67.1	13.8

detected by comparing results of Tables 3 and 4. However, those differences can easily be corrected by adjusting the composition and/or firing conditions.

This is a good indication of the irrelevant role of minor components in the development of major phases, despite its expectable crucial effect on the refractoriness of sintered materials. This clearly demonstrates the potential of the use of wastes in ceramic formulations of industrial interest.

4. Conclusions

Detailed characterisation studies show that the combination of several industrial wastes and conventional ceramic procedures is a promising way to produce refractory and cement-type materials. The use of the equilibrium phase diagram of the relevant system helps defining suitable compositions and processing conditions. Two main classes of materials can be considered: (i) refractories (based on CA_6); and (ii) cements (containing C_3A, $C_{12}A_7$, C_2S phases). The presence of impurities in the waste materials induces changes on functional properties (e.g. mechanical resistance and refractoriness), since they accelerate the sintering process and reactions between the constituents. As a consequence, C1 and C3 sintered samples show better properties than the corresponding C1-P and C3-P standard samples. However, those differences can easily be accounted for.

Acknowledgement

Financial support by CAPES–MEC, Brazil, is greatly appreciated (F. Raupp-Pereira, Ph.D. grant).

References

[1] J.M.F. Ferreira, P.M.C. Torres, M.S. Silva, J.A. Labrincha, Recycling of sludges generated from natural stones cutting processes in ceramic formulations, in: B. Bjorkman, C. Samuelsson, J. Wikstrom (Eds.), Proceedings of the TMS Fall Meeting on Recycling and Waste Treatment in Mineral and Metal Processing: Technical and Economic Aspects, vol. 2, Lulea, Sweden, 2002, pp. 389–395.
[2] M.J. Ribeiro, D.U. Tulyaganov, J.M.F. Ferreira, J.A. Labrincha, Recycling of Al-rich industrial sludge in refractory ceramic pressed bodies, Ceram. Int. 28 (2002) 319–326.
[3] F.R. Pereira, A.F. Nunes, A.M. Segadães, J.A. Labrincha, Refractory mortars made of different wastes and natural sub-products, Key Eng. Mater. 264–268 (2004) 1743–1746.
[4] D.U. Tulyaganov, S.M.H. Olhero, M.J. Ribeiro, J.M.F. Ferreira, J.A. Labrincha, Mullite-alumina refractory ceramics obtained from mixtures of natural common materials and recycled Al-rich anodizing sludge, J. Mater. Synth. Proc. 10 (2002) 311–318.
[5] D.A. Pereira, D.M. Couto, J.A. Labrincha, Incorporation of aluminum-rich residues in refractory bricks, Ceram. Forum Int. 77 (2000) 21–25.
[6] M.J. Ribeiro, J.M.F. Ferreira, J.A. Labrincha, Clay-based ceramic formulations containing different solid wastes, Euroceram. Newslett. 14 (2002) 4–7.
[7] E. Martelon, J. Jarrige, M.J. Ribeiro, J.M.F. Ferreira, J.A. Labrincha, New clay-based ceramic formulations containing different solid wastes, Ind. Ceram. 20 (2000) 71–76.
[8] J.A. Perez, R. Terradas, M.R. Manent, M. Seijas, S. Martinez, Inertization of industrial wastes in ceramic materials, Ind. Ceram. 16 (1996) 7–10.
[9] M. Dondi, M. Marsigli, B. Fabbri, Recycling of industrial and urban wastes in brick production—a review, Tile Brick Int. 13 (1997) 302–308.
[10] S. Pinto, K. Rosenbom, L. Machado, J.A. Labrincha, V.M. Ferreira, Incorporation of sludges in light expanded clay aggregates, Key Eng. Mater. 264 (2004) 1391–1394.
[11] D.A. Pereira, J.B. Aguiar, F.P. Castro, M.F. Almeida, J.A. Labrincha, Mechanical behaviour of portland cement mortars with incorporation of Al-rich salt slags, Cement Concrete Res. 30 (2000) 1131–1138.
[12] F.R. Pereira, D. Hotza, A.M. Segadães, J.A. Labrincha, Recycling of Several Wastes as Refractory Materials, in: Proceedings of the UNITECR'03, TARJ, Osaka, Japan, 2003, pp. 150–153.
[13] T. Maruta, H. Ohmori, M. Moriya, K. Uchida, H. Isoda, Properties of the soil improved by the special cement made from municipal solid waste incineration ashes, Inorg. Mater. 4 (1997) 152–155.
[14] M. Kawamura, K. Torii, Chloride permeability of concrete containing a fly ash and a blast furnace slag, Mater. Res. Soc. Symp. Proc. 137 (1989) 411–416.
[15] A. Samarin, Hydraulic cements—new types and raw materials and radically new manufacturing methods, in: R.K. Dhir, M.J. McCarthy (Eds.), Proceedings of the International Conference—Volume on Appropriate Concrete Technologies, University of Dundee, E&F.N. Spon, London, 1997, pp. 265–279.
[16] W.D. Gluchowski, W. Zajtsew, W. Pachomow, Slag-alkaline cements and concrete; structures, properties, technological and economical aspects of use, Silic. Ind. 48 (1983) 197–200.
[17] P. Nunes, M.J. Ribeiro, J.M.F. Ferreira, C.S. Bóia, J.A. Labrincha, Mullite-based materials obtained from industrial wastes and natural sub-products, in: B. Bjorkman, C. Samuelsson, J. Wikstrom (Eds.), Proceedings of the TMS Fall Meeting on Recycling and Waste Treatment in Mineral and Metal Processing: Technical and Economic Aspects, vol. 2, Lulea, Sweden, 2002, pp. 359–368.
[18] A.M. Seabra, D.A. Pereira, C.M. Bóia, J.A. Labrincha, Pre-treatment needs for the recycling of Al-rich anodising sludge as a ceramic raw material, in: C.S. Gomes (Ed.), Proceedings of the 1st Latin American Clay Conference, vol. 2, Portuguese Clay Society, Funchal, Portugal, 2000, pp. 176–181.